Waveform Design for Vital Signs Detection in Integrated Sensing and Communication System

Chi Zhang[1], Yongwei Zhang[1], Delong Xing[1], Murat Temiz[2]
[1]School of Transportation and Civil Engineering, Nantong University, Nantong, Jiangsu 226019, China
[2]Department of Electronic and Electrical Engineering, University College London, WC1E 7JE, London, UK
*Corresponding author: Yongwei Zhang (david.y.zhang@ntu.edu.cn)
Emails: zhangchi1845@stmail.ntu.edu.cn, david.y.zhang@ntu.edu.cn, xdl@ntu.edu.cn, m.temiz@ucl.ac.uk

***Abstract*—The integration of sensing and communication functions in one platform has become a pivotal use case in future communication systems. This research investigated the optimal integrated sensing and communication (ISAC) waveforms for the purpose of vital signs detection. In order to incorporate both functions in the system and make it favorable for sensing the micro-doppler effect associated with vital signs, orthogonal frequency division multiplexing (OFDM) and phase-coded frequency modulated continuous wave (PC-FMCW) signals were adopted and compared, and the performances were evaluated against the system based on the classic frequency modulated continuous wave (FMCW). Several phase coded FMCW signals have been investigated and the simulated results indicated that the Frank-coded PC-FMCW waveform exhibited an optimal performance for vital signs detection in a line-of-sight setting. The work is beneficial for search and rescue applications where high-performance sensing such as vital signs detection and limited communication capability is required.**

***Index Terms*—Integrated sensing and communication, Line-of-sight, Multipath, OFDM, Phase-coded FMCW**

I. Introduction

VITAL sign monitoring serves as a cornerstone of modern healthcare, enabling early diagnosis of cardiovascular abnormalities, respiratory disorders, and metabolic imbalances through continuous tracking of heart rate, breathing patterns, and body movement characteristics. In both clinical and home care settings, millimeter-wave radar systems have emerged as non-contact alternatives to wearable sensors, maintaining measurement accuracy while eliminating skin irritation risks. Conventional radar architectures encounter fundamental limitations in line-of-sight (LOS) multipath environments—prevalent in urban canyons and confined indoor spaces—manifested through prohibitive hardware costs, system complexity, reliance on millimeter-wave frequencies, and excessive bandwidth demands [1], [2]. These constraints exacerbate power consumption and form-factor challenges, critically hindering scalable deployment in clinical telemonitoring and consumer homecare applications.

Integrated Sensing and Communication (ISAC) systems strategically overcome these barriers via shared hardware platforms and dynamic spectrum utilization, enabling resource-efficient joint functionality [3], [4]. Among the ISAC-compatible waveforms, orthogonal frequency division multiplexing (OFDM) and phase-coded frequency modulated continuous wave (PC-FMCW) have shown advantages in vital signs detection. OFDM takes advantage of the quadrature and cyclic prefixes of subcarriers to effectively suppress inter-symbol interference (ISI) in dense multipath channels [5]. On the other hand, FMCW signals can also be used to develop radar-centric ISAC systems [6], [7]. PC-FMCW utilizes phase-coded chirp signals to achieve interference suppression when multiple radars exist in the area [8], [9]. The question of which waveform is better suited for vital signs detection applications remains unresolved. However, optimizing waveforms faces several key challenges. There is a lack of unified experimental frameworks to directly compare their performance under realistic line-of-sight (LOS) multipath conditions. Then, insufficient analysis exists regarding the time-frequency resolution trade-offs that critically affect the discrimination of cardiopulmonary signals. These knowledge gaps collectively prevent the development of robust, energy-efficient contactless monitoring systems capable of meeting clinical-grade reliability standards for next-generation healthcare.

This research investigated the optimal ISAC waveforms for the purpose of vital sign detection within line-of-sight multipath scenarios. In this paper, an LOS multipath model with vital signs effects was developed and validated by simulations of typical indoor environments. Using the traditional FMCW as a benchmark, we performed vital sign detection by using both PC-FMCW (with 6 different codes) and OFDM signals. Mean square error (MSE) quantifies waveform performance in a controlled multipath configuration. More than 100 trials performed under the same channel conditions ensured statistical significance. This work provides critical design for ISAC waveform in 5G/6G medical systems operating in complex electromagnetic environments.

II. System Model

This section presents the system model employed in this study. The complete model architecture is illustrated in Fig. 1.

A. Transmitted Signal Model

The transmitted signal uses OFDM and PC-FMCW waveforms.

This work was supported in part by the NSFC under Grants 62361136811, 62174091, and 62201294, TUBITAK Grant 123N800, and METU BAP Grant AGEP-301-2025-11558.

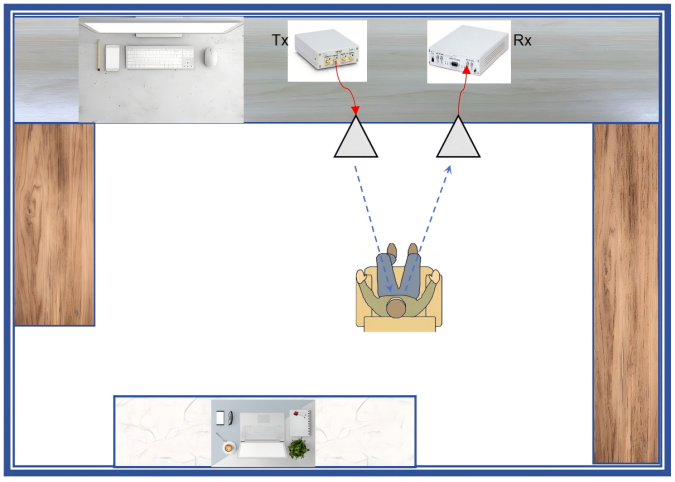

Fig. 1: The conceptual setup of the ISAC system for vital signs detection, the Tx and Rx moddules are colocated and synchronized.

1) OFDM Signal: OFDM waveforms demonstrate superior flexibility for both sensing and communications compared to alternative dual-functional modulated signals [10], making them particularly suitable for ISAC applications. The complex baseband time-domain OFDM signal is formulated as [11],

$$s(t) = \sum_{m=0}^{M-1} \sum_{k=0}^{N_c-1} X_{m,k} e^{j2\pi k \Delta f (t - mT_{\text{sym}})} \cdot \text{rect}\left(\frac{t - mT_{\text{sym}}}{T_s}\right), \tag{1}$$

where M represents the total number of OFDM symbols in a time frame, N_c denotes the total number of subcarriers, and $X_{m,k} \in \mathbb{C}$ corresponds to the complex modulation symbol allocated to the k-th subcarrier of the m-th OFDM symbol. The subcarrier spacing and symbol duration are denoted by Δf and T_s, respectively, and $\Delta f = 1/T_s$. Each symbol extends to $T_{\text{sym}} = T_s + T_{\text{cp}}$ through cyclic prefix insertion, where T_{cp} denotes the guard interval duration. The rectangular window function $\text{rect}(\tau)$ satisfies $\text{rect}(\tau) = 1$ for $0 \leq \tau < 1$ and $\text{rect}(\tau) = 0$ otherwise, ensuring strict temporal confinement of individual OFDM symbols.

2) PC-FMCW Signal: The PC-FMCW signal combines linear frequency modulation (chirp) with various phase coding sequences. Within each chirp duration T_{chirp}, the transmitted PC-FMCW signal is expressed as,

$$s_{\text{PC}}(t) = \sum_{n=0}^{N_{\text{chirp}}-1} c_n \exp\left(j2\pi\left(f_c t + \frac{B}{2T_{\text{chirp}}} t^2\right)\right), \tag{2}$$

where f_c is the carrier frequency (2.4 GHz), B is the bandwidth (1 MHz), and N_{chirp} is the number of chirps determined by the simulation duration and chirp duration (20 ms). Specifically, the phase codes c_n employed include:

- **Barker codes:** Known for minimal sidelobes, beneficial for clear signal detection. The Barker code of length 7 is given by
$$[1, 1, 1, -1, -1, 1, -1]. \tag{3}$$
- **Golomb codes:** Offer favorable autocorrelation properties enhancing signal robustness, typically generated from primitive polynomials. The length utilized here is 11.
- **Gold codes:** Exhibit strong cross-correlation resistance, reducing interference in multipath scenarios. A Gold code of length 31 is applied, constructed from two preferred m-sequences.
- **Costas codes:** Provide optimal ambiguity function characteristics suitable for radar ranging and Doppler detection. A Costas array of length 7 is adopted.
- **Frank codes:** Possess superior Doppler resolution properties, generated by arranging elements into an $L \times L$ matrix, given by,
$$F(m,n) = \exp\left(j\frac{2\pi}{L}mn\right), \quad m,n = 0,1,...,L-1. \tag{4}$$
Here, the Frank code with size $L = 4$ is utilized.
- **Zadoff-Chu codes:** Characterized by ideal periodic autocorrelation, minimizing interference. The Zadoff-Chu sequence used is defined as,
$$ZC(n) = \exp\left(-j\pi u \frac{n(n+1)}{N}\right), \quad n = 0,1,...,N-1 \tag{5}$$
with parameter $u = 1$ and length $N = 13$.

B. Line-of-Sight Multipath Channel Model

Figure 1 illustrates the measurement setup for the heartbeat and respiration scenario, which is equipped with a single transmit antenna and a single receive antenna. The channel model of this setup can be modeled as a multi-path channel, where the propagation path is influenced by respiration and heartbeat, such that Doppler shifts are introduced to the reflected signal due to the respiration and heartbeat of the target. The multipath channel impulse response is given by [12],

$$\mathbf{H}(t,\tau) = \sum_{l=1}^{L} b_l \delta(t - \tau_l) e^{-j(2\pi f_{D,l} t + \varphi_l)}, \tag{6}$$

where L is the total number of multi-path components, with each path l having complex amplitude b_l and propagation delay τ_l, and $\delta()$ is the impulse response. The Doppler shift $f_{D,l} = 2v_l f_c/c$ results from target radial velocity v_l, where f_c is the carrier frequency and c is the speed of light, φ_l is the phase variation of the l_{th} path.

The chest movement-induced phase due to the heartbeat and respiration is modeled as [13],

$$\varphi(t) = \frac{4\pi d_0}{\lambda} + \frac{4\pi x(t)}{\lambda} - \varphi_1\left(t - \frac{2d_0}{c}\right), \tag{7}$$

where d_0 represents the nominal distance to the thorax and λ is wavelength. $x(t) = A_r \cos(\omega_r t) + A_h \cos(\omega_h t)$ models the time-varying chest displacement, where A_r and A_h represent amplitudes of respiratory and cardiac displacement, with the angular frequencies $\omega_r = 2\pi f_r$ and $\omega_h = 2\pi f_h$ corresponding to the rates of breathing and heartbeat. The term $\varphi_1(\cdot)$ accounts for phase perturbations during signal

propagation, incorporating effects of tissue heterogeneity and environmental factors. Assuming that the line-of-sight (LOS) path carries the heartbeat and respiration information due to the LOS measurement setup, including the micro-Doppler effects induced by the heartbeat and respiration, the modified channel model becomes

$$\begin{aligned}\mathbf{H}(t,\tau) = \; & b_1\delta(t-\tau_1)\cdot \\ & \exp\!\left(-j2\pi f_{D,1}t - j\frac{4\pi}{\lambda}(d_0+x(t)) - j\varphi_1\!\left(t-\frac{2d_0}{c}\right)\right) \\ & + \sum_{l=2}^{L} b_l\delta(t-\tau_l)\exp\left(-j\left(2\pi f_{D,l}t-\phi_l\right)\right),\end{aligned} \tag{8}$$

where $\tau_1 = 2d_0/c$ represents the round-trip delay, and $\phi_l(t)$ captures both static phase offset and time-varying perturbations of the lth path. The time-varying phase disturbance $\phi_1(t)$ introduces nonlinear distortions from environmental perturbations and tissue dielectric variations.

C. Time-Domain Received Signal

The baseband received signal incorporating both vital sign modulation and environmental multipath effects is formulated as,

$$r(t) = \int_{-\infty}^{\infty} \mathbf{H}(t,\tau)s(t-\tau)d\tau + n(t), \tag{9}$$

where $\mathbf{H}(t,\tau)$ represents the time-varying channel impulse response defined in (8), $s(t)$ denotes the transmitted waveform, and $n(t) \sim \mathcal{CN}(0,\sigma_n^2)$ denotes the complex additive white Gaussian noise (AWGN) with noise variance σ_n^2. Due to the first term of the channel model, corresponding to the LOS path, given by (8), the received signal $r(t)$ contains the vital sign information through chest displacement modeled by $x(t) = A_r\cos(\omega_r t) + A_h\cos(\omega_h t)$.

III. Experimental Procedure

To ensure the effectiveness of the experiment, this study constructs a verification framework from three core dimensions: firstly, the real environment characteristics are constructed through the coupled multipath attenuation model, and the actual propagation scenario of weak direct signal and complex multipath reflection is accurately simulated; Secondly, based on the carrier phase modulation mechanism of submillimeter thoracic motion, the small physiological displacement is converted into the carrier phase shift, which requires the system to have high-precision phase tracking ability to capture subtle changes. At the same time, the standardized 100Hz uniform downsampling rate and second-order Butterworth filter parameter configuration are used to ensure the data comparability between different experimental protocols. The framework strikes a balance between theoretical rigor and engineering achievability and provides a scientific benchmark for cross-scenario performance evaluation through systematic technical path design. Key system parameters utilized in the simulation and analysis are summarized in Table I.

TABLE I: System Parameters and Configurations

Parameter	Value	Unit	Description
Basic System Parameters			
f_s	1	MHz	Sampling rate
f_c	2.4	GHz	Carrier frequency
T_{total}	30	s	Total simulation time
N_{paths}	5	–	Number of multipath components
OFDM Parameters			
N_{sub}	64	–	Number of subcarriers
N_{cp}	16	–	Cyclic prefix length
T_{sym}	80	μs	OFDM symbol duration
D_{pilot}	10	symbols	Pilot insertion interval
M_{QAM}	4	–	QAM modulation order
PC-FMCW Parameters			
T_{chirp}	80	μs	Chirp duration
B	1	MHz	Chirp bandwidth
K	12.5	MHz/μs	Chirp slope
N_{chirps}	125	–	Number of chirps per frame
Vital Sign Parameters			
f_{resp}	0.2	Hz	Respiration frequency
f_{heart}	1.0	Hz	Heartbeat frequency
Δd_{resp}	10	mm	Chest displacement (respiration)
Δd_{heart}	2	mm	Chest displacement (heartbeat)
Receiver Processing			
N	100	–	Total iteration number
$f_{s,\text{ds}}$	100	Hz	Downsampling rate
N_{filt}	2	–	Butterworth filter order
BW_{resp}	[0.15, 0.5]	Hz	Respiration bandpass range
BW_{heart}	[0.8, 2]	Hz	Heartbeat passband range
N_{FFT}	1024	–	FFT size for spectral analysis

A. Signal Generation and Modulation

The experiment involves generating and processing two types of wireless signals: **OFDM** and **Phase-coded FMCW (PC-FMCW)**, with classical FMCW serving as a baseline. The signal generation process is structured as follows:

For OFDM signals, a 64-subcarrier configuration is adopted, with a cyclic prefix length of 16 and a total of 15,625 symbols calculated dynamically for a 30-second simulation. Pilot symbols composed of all-ones sequences are inserted every 10 symbols to facilitate channel estimation. Data streams are modulated using QPSK and mapped to non-pilot subcarriers. Time-domain waveforms are generated through the IFFT, followed by cyclic prefix insertion to mitigate multipath delay spread. Transmit power is normalized to 1.0 via standard deviation scaling to ensure fair comparison.

PC-FMCW signals are constructed using linear frequency-modulated chirp pulses (80μs duration, 1 MHz bandwidth) with six coding schemes: Barker7, Golomb11, Gold31, Costas7, Frank codes, and Zadoff-Chu codes. Each chirp pulse is phase-modulated cyclically using these sequences. For instance, Frank codes generate orthogonal frequency matrices for phase transitions, while Zadoff-Chu codes leverage constant envelope-zero autocorrelation properties for multipath suppression. The frame structure ensures integer multiples of chirp pulses per coding period for complete sequence

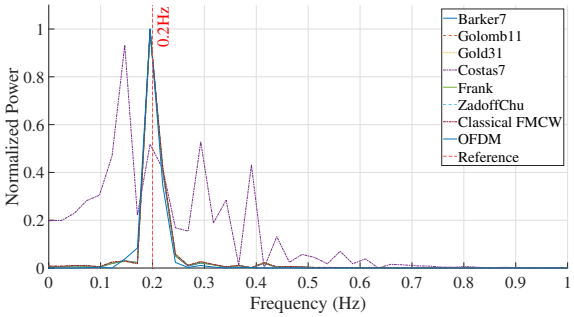

Fig. 2: The estimated respiration response in the frequency domain after applying the passband filter (0.1-0.5 Hz).

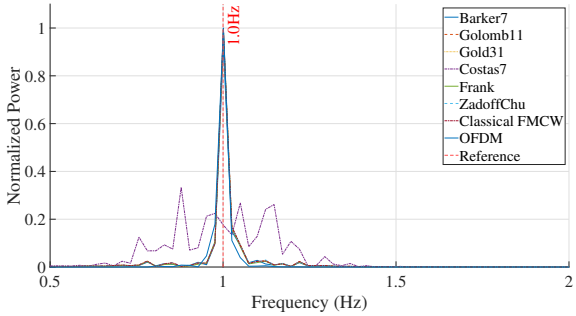

Fig. 3: The estimated heartbeat response in the frequency domain after applying the passband filter (0.8-2 Hz).

coverage. Classical FMCW signals are generated using identical chirp parameters but omit phase coding, serving as a performance benchmark.

B. Signal Processing

OFDM demodulation begins with cyclic prefix correlation for symbol synchronization. After FFT-based subcarrier demapping, continuous phase variations are extracted via unwrapped arctangent operation $\phi(t) = \text{unwrap}(\angle r(t))$. Downsampling to 100 Hz precedes bandpass filtering (0.15–0.5 Hz for respiration, 0.8–1.2 Hz for cardiac signals).

PC-FMCW processing employs Hilbert transform-derived analytic signals for phase extraction $\phi(t) = \text{unwrap}(\angle \mathcal{H}(r(t)))$. Coherent accumulation across chirp periods enhances SNR before identical downsampling and filtering. Classical FMCW skips phase decoding but shares subsequent processing steps. All extracted signals undergo amplitude normalization to eliminate scaling discrepancies, with strict temporal alignment to reference sinusoids (0.2 Hz and 1.0 Hz) for error-free metric computation.

C. Performance Evaluation Metrics

The Mean Squared Error (MSE) measures the average squared difference between the estimated vital sign frequencies and the ground truth frequencies associated with vital signs. 100 iterations have been simulated for generalization. It is calculated as:

$$\text{MSE}_{\text{resp}} = \frac{1}{N}\sum_{k=1}^{N}\left(f_{k,1} - f_{\text{resp}}\right)^2, \tag{10}$$

$$\text{MSE}_{\text{heart}} = \frac{1}{N}\sum_{k=1}^{N}\left(f_{k,2} - f_{\text{heart}}\right)^2, \tag{11}$$

where $f_{k,1}$ is the estimated frequency for respiration in the kth iteration, and $f_{k,2}$ is the estimated frequency for heartbeat in the kth iteration, f_{resp} and f_{heart} are the baseline frequency for respiration and heartbeat respectively, N is the total iteration number.

IV. Results

The received time domain signal was transformed into the frequency domain first. Then, two passband filters were applied to investigate the vital signs characterized by two baseline frequencies. Fig. 2 shows the signal after the lower passband (0.1-0.5 Hz) was applied, whereas Fig. 3 illustrates the signal after applying the higher passband filter (0.8-2 Hz).

It is observed in Fig. 2 that all signals after the low passband filter showed a peak at the baseline frequency of 0.2 Hz, which coincides with frequency of the baseline respiratory signal. The received signal based on Barker7 coding displayed the narrowest bandwidth among all waveforms. However, it does not translate into an obvious advantage for frequency determination compared with other waveforms such as Frank coding and OFDM. On the other hand, the received singal based on Costas7 coding exhibited some substantial harmonic components, few secondary spectrum peaks being observed. These harmonics may affect the vital signs detection as their spacing in frequency is close. It appears that the FMCW system with the Costas7 coding gave the worst performance for respiratory sign determination.

As observed in Fig. 3, all signals after applying the high passband filter except those using Costas7 coding exhibited a main peak at 1.0 Hz, a baseline frequency for the heartbeat response. Similarly to the respiratory, the filtered signal based on the Costas7 coding showed few harmonics, which may obscure the main peak related to heartbeat sign determination. The existence of secondary spectrum peaks in the received signal makes it a chanllenge to make accurate estimation for vital signs detection.

As observed in Fig.4, which presents the MSE of estimated vital signs frequency in comparison to the hypothesis frequencies of vital signs by adopting various waveforms for sensing. It is shown that Frank-coded FMCW achieved the lowest MSE, followed by Barker7-coded FMCW. On the other hand, Costas7-coded FMCW has the highest MSE, and OFDM showed the second highest MSE. These findings suggest that Frank-coded FMCW waveforms are favorably suited for vital signs detection applications, followed by Barker coding. It is noted that the system based on OFDM where random signals were modulated onto subcarriers.

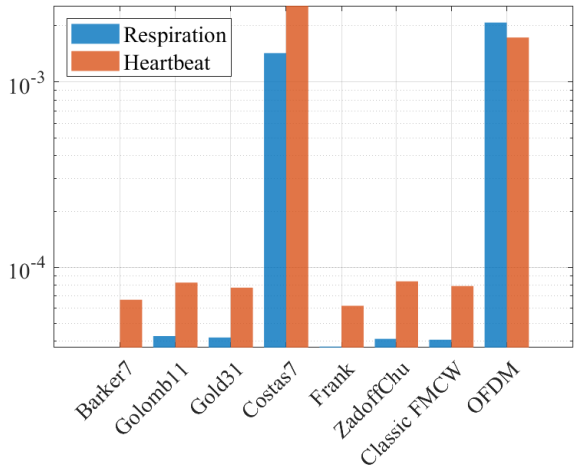

Fig. 4: MSE of estimated vital signs frequency in comparison to the hypothesis baseline frequencies of vital signs by adopting various waveforms for sensing. The baseline frequency for respiratory is 0.2 Hz and 1 Hz for heartbeat.

V. Conclusion

This study explores various ISAC waveforms for vital signs detection. OFDM and PC-FMCW signals were adopted in the established scenario for sensing performance evaluation, PC-FMCW signals were optimized via phase-coding and the obtained performance were compared against the classic FMCW and OFDM-based systems. Numerical simulations indicated that Frank-coded PC-FMCW signals is most promising for vital signs detection, whereas OFDM waveforms showed only moderate performance for sensing. It demonstrated that the PC-FMCW signals are favorable for micro-Doppler determination compared with conventional FMCW or OFDM signals. The simulation study was based on a line-of-sight setting with only one human subject being considered, and the communication function was not investigated. In future research, multi-targets with motion interference under non-line-of-sight conditions and communication capability will be examined together.

References

[1] J. Jung, S. Lim, J. Kim and S. -C. Kim, "Non-Line-of-Sight Vital Sign Detection Using Multipath Propagation of UWB Radar," in IEEE Antennas and Wireless Propagation Letters, vol. 23, no. 7, pp. 2219-2223, July 2024, doi: 10.1109/LAWP.2024.3386177.

[2] L. Kouhalvandi and S. Karamzadeh, "Advances in Non-Contact Human Vital Sign Detection: A Detailed Survey of Radar and Wireless Solutions," in IEEE Access, vol. 13, pp. 27833-27851, 2025, doi: 10.1109/ACCESS.2025.3540716.

[3] Z. Du, F. Liu, Y. Xiong, T. X. Han, Y. C. Eldar and S. Jin, "Reshaping the ISAC Tradeoff Under OFDM Signaling: A Probabilistic Constellation Shaping Approach," in IEEE Transactions on Signal Processing, vol. 72, pp. 4782-4797, 2024, doi: 10.1109/TSP.2024.3465499.

[4] F. Liu, C. Masouros, A. P. Petropulu, H. Griffiths and L. Hanzo, "Joint Radar and Communication Design: Applications, State-of-the-Art, and the Road Ahead," in IEEE Transactions on Communications, vol. 68, no. 6, pp. 3834-3862, June 2020, doi: 10.1109/TCOMM.2020.2973976.

[5] K. Wu, J. A. Zhang, X. Huang and Y. J. Guo, "Integrating Low-Complexity and Flexible Sensing Into Communication Systems," in IEEE Journal on Selected Areas in Communications, vol. 40, no. 6, pp. 1873-1889, June 2022, doi: 10.1109/JSAC.2022.3156649.

[6] M. Temiz, N. J. Peters, C. Horne, M. A. Ritchie and C. Masouros, "Radar-Centric ISAC Through Index Modulation: Over-the-air Experimentation and Trade-offs," 2023 IEEE Radar Conference (RadarConf23), San Antonio, TX, USA, 2023, pp. 1-6, doi: 10.1109/RadarConf2351548.2023.10149620.

[7] M. Temiz, C. Horne, N. J. Peters, M. A. Ritchie and C. Masouros, "An Experimental Study of Radar-Centric Transmission for Integrated Sensing and Communications," in IEEE Transactions on Microwave Theory and Techniques, vol. 71, no. 7, pp. 3203-3216, July 2023, doi: 10.1109/TMTT.2023.3234309.

[8] F. Uysal, "Phase-Coded FMCW Automotive Radar: System Design and Interference Mitigation," in IEEE Transactions on Vehicular Technology, vol. 69, no. 1, pp. 270-281, Jan. 2020, doi: 10.1109/TVT.2019.2953305.

[9] T. Elazar and E. Socher, "A 90-98 GHz CMOS Transmitter Frontend for Concurrent Phase-Coded FMCW Radar Applications," in IEEE Journal of Microwaves, vol. 2, no. 2, pp. 275-285, April 2022, doi: 10.1109/JMW.2022.3154924.

[10] C. Zhang, J. Duan, S. Lu, D. Zhang, M. Temiz, Y. Zhang, and Z. Meng, "Design and Experimental Demonstration of an Integrated Sensing and Communication System for Vital Sign Detection," Sensors, vol. 25, p. 3766, 2025, doi: 10.3390/s25123766.

[11] C. Sturm and W. Wiesbeck, "Waveform Design and Signal Processing Aspects for Fusion of Wireless Communications and Radar Sensing," in Proceedings of the IEEE, vol. 99, no. 7, pp. 1236-1259, July 2011, doi: 10.1109/JPROC.2011.2131110.

[12] J. A. Zhang, X. Huang, Y. J. Guo, J. Yuan and R. W. Heath, "Multibeam for Joint Communication and Radar Sensing Using Steerable Analog Antenna Arrays," in IEEE Transactions on Vehicular Technology, vol. 68, no. 1, pp. 671-685, Jan. 2019, doi: 10.1109/TVT.2018.2883796.

[13] Apriono, Catur, Fathul Muin, and Filbert H. Juwono. 2021. "Portable Micro-Doppler Radar with Quadrature Radar Architecture for Non-Contact Human Breath Detection" Sensors 21, no. 17: 5807. https://doi.org/10.3390/s21175807